Urs Baltensperger
Paul Scherrer Institute
CH Villigen

Measurement of the Hydrophilic Behavior of Soot

Measurement of the Hydrophilic Behavior of Soot

Urs Baltensperger
Paul Scherrer Institute
CH-5232 Villigen PSI

Workshop on Combustion Particle Measurement,
ETH Zürich, 7 August, 1997

Importance of the surface characteristics of aerosol particles

- Health effects
- Reactive surface area for atmospheric chemistry
- Response to high relative humidity (behavior in a cloud; residence time in the atmosphere)

Tools to probe the surface of aerosol particles

- Secondary neutral mass spectrometry (SNMS) and secondary ion mass spectrometry (SIMS)
- X-ray excited photoelectron spectroscopy (XPS)
- Photoelectric aerosol sensor
- Tandem DMA for the investigation of the hydrophilic behavior of the aerosol particles

Possible reasons for increasing hygroscopicity with aging time:

- Coagulation with water soluble particles
- Gas to particle conversion (heterogeneous nucleation), e.g. as a result of photochemical gas phase reactions (example: addition of ozone to diesel exhaust gas, Weingartner et al., Atmos. Environ. 31, 2311 (1997))
- Adsorption and reaction of gaseous molecules (example: NO_2 adsorption to carbonaceous aerosols, see below)
- (Photo)-chemical degradation of aerosol particle surface (example: Photodegradation of nitro-PAHs, see below)
- Cloud processing

Reaction of NO_2 with soot particles:

- Formation of nitric acid:

$$2\ NO_2 + H_2O = HNO_{3\ ads} + HONO$$

- Oxidation of soot surface by formation of HONO:

$$NO_2 + red_{ads} \xrightarrow{H_2O} HONO\ (g) + ox_{ads}$$

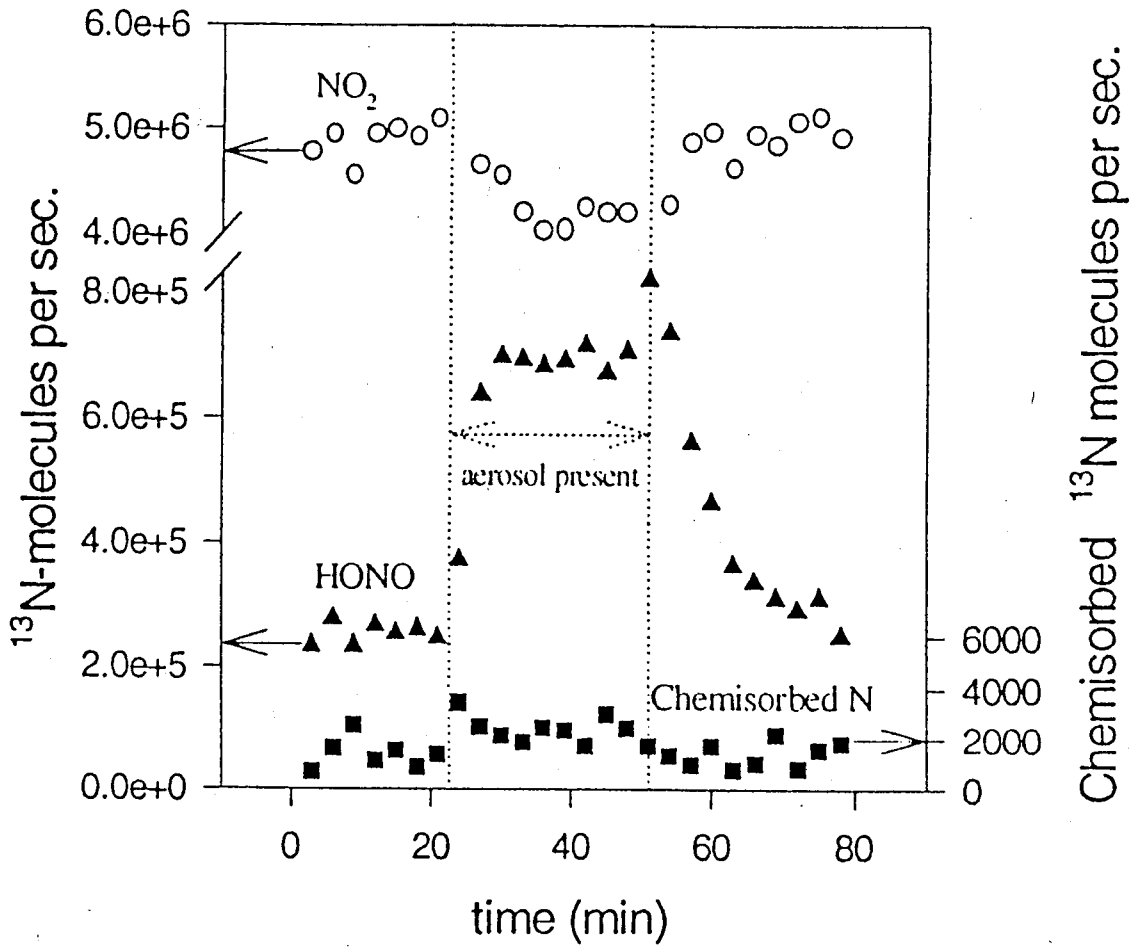

Ammann et al., submitted to Nature (1997)

Photodegradation of nitro-PAHs on diesel soot particles results in half-lives of about 1 hour at noon

(Fan et al., ES&T 30, 1358 (1996)

What are the products?

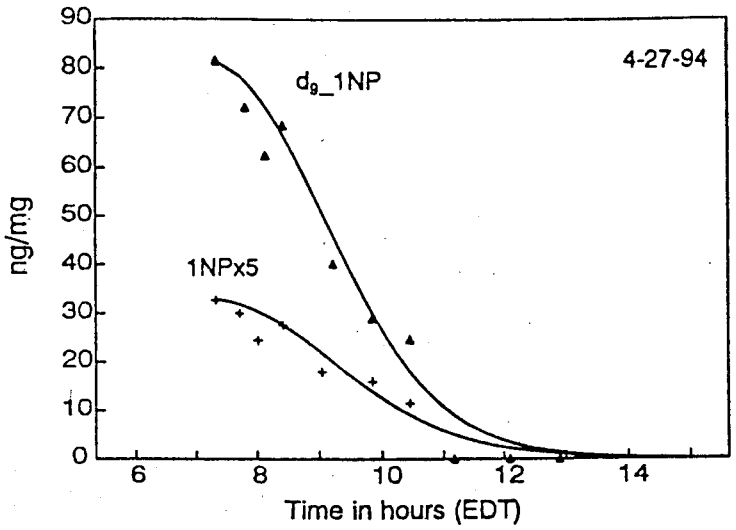

FIGURE 4. Simulation (solid line) and data (symbols) of 1NP and d_9-1NP decay on diesel soot in sunlight ($k_{1NP} = 0.030 \pm 0.005 k_{NO_2}$, April 27, 1994). The photolysis rate of PAH was referenced to that of NO_2 in order to relate the observed decay of NPAH to the changing solar irradiation.

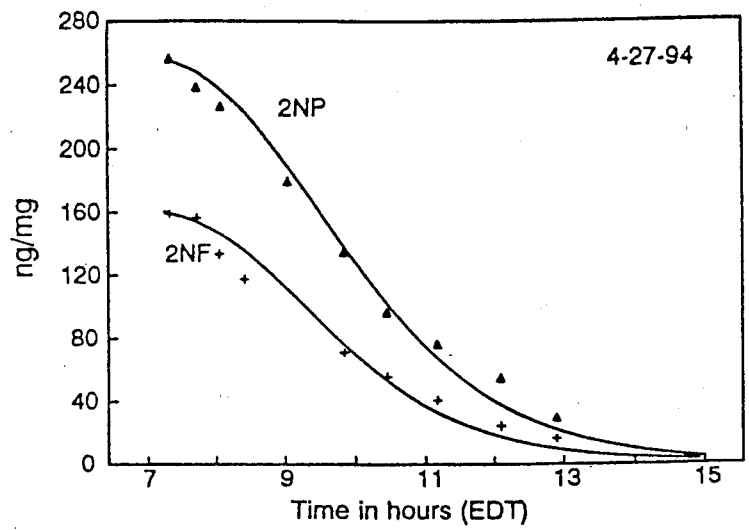

FIGURE 5. Simulation (lines) and data (symbols) of 2NF and 2NP decay on diesel soot in sunlight (April 27, 1994).

The formation of new small particles behind particles filters of diesel engines can be explained as follows: cooling of the exhaust gas behind the filter results in condensation of semi-volatile material. Without a particle filter, this material would condense on the diesel soot particles. Since the mass of this material is very small, this condensation does not necessarily result in a measurable increase of the diameter of the diesel particles. With the particle filter, the original particles are removed so that the condensation results in the formation of new particles.

This nicely demonstrates the complex interplay between homogeneous and heterogeneous nucleation: homogeneous nucleation, i.e., the formation of new particles requires a certain supersaturation, since very small particles are unstable. In the presence of a high surface area of already existing particles, the condensable molecules rapidly attach to these particles (called heterogeneous nucleation). This process reduces the life-time of the condensable species so that the concentration required for a critical supersaturation may not be reached.

U. Baltensperger

Pergamon

Atmospheric Environment Vol. 31, No. 15, pp. 2311–2327, 1997

1352–2310/97 $17.00 + 0.00

PII: S1352–2310(97)00023–X

HYGROSCOPIC PROPERTIES OF CARBON AND DIESEL SOOT PARTICLES

E. WEINGARTNER,*† H. BURTSCHER* and U. BALTENSPERGER†‡

* Laboratory for Solid State Physics, ETH, 8093 Zürich, Switzerland; and † Paul Scherrer Institute, 5232 Villigen PSI, Switzerland

(*First received* 10 *July* 1996 *and in final form* 28 *November* 1996. *Published May* 1997)

Abstract—Laboratory experiments were performed in order to study the hygroscopic properties of freshly produced carbon and diesel soot particles at subsaturations (i.e. at relative humidity < 100%). Wetted carbon aggregates collapsed to a more compact structure. In contrast, the diesel combustion particles exhibited a much smaller restructuring combined with condensational growth. The hygroscopicity of the diesel particles was enhanced when the sulfur content of the fuel was increased or when the particles were subjected to an ozone and UV pre-treatment. By extrapolating the data with a Köhler model critical supersaturations were calculated. Freshly emitted combustion particles are unlikely to act as cloud condensation nuclei whereas an aging of the particles will enhance their nucleation ability. © 1997 Elsevier Science Ltd.

Key word index: Combustion aerosols, soot, hygroscopic properties, TDMA, capillary condensation, condensational growth.

1. INTRODUCTION

Once emitted into the atmosphere combustion particles will undergo several aging processes. Not much is known about the nucleation properties of freshly emitted or aged soot particles. The hygroscopicity of aerosol particles has an important influence on their residence time in the atmosphere as well as on their optical properties. The absorption of solar radiation by soot particles is increased if the particles are incorporated into cloud droplets (Chylek and Hallett, 1992). This process leads to a decrease of the cloud albedo. In contrast, if soot particles act as cloud condensation nuclei (CCN) (i.e. act as nuclei for the condensation of cloud droplets) they can increase the cloud albedo by changing the droplets size distribution towards smaller droplets (Twomey *et al.*, 1984). These effects may influence the global energy balance and they are important for visibility degradation. Furthermore, the hygroscopicity of atmospheric particles is important for their chemical behavior (aqueous-phase chemical reactions).

The response of an aerosol particle to relative humidity (RH) depends on the following properties:

(a) *Size and solubility of the particle.* The water pressure above a water droplet containing dissolved material is lowered by the Raoult effect. The size and the fraction of soluble material in an aerosol particle will determine at which supersaturation it will be activated and thus will form a cloud droplet. The equilibrium size of a droplet was first described by Köhler (1936), who considered the Raoult (solute) effect and the Kelvin (curvature) effect.

(b) *Wetability and structure of the surface.* Water can partially wet a completely water insoluble particle with an irregular shape. The curvature of the liquid water surface in small angle capillaries depends on the contact angle Θ between the water surface and solid surface where Θ is measured inside the liquid (Young's relation, see Myers, 1991). A surface that is readily wetted by water is called hydrophilic and is characterized by small contact angles. For $\Theta > 90°$ (highly hydrophobic particles), the curvature of the water surface is positive and it is in equilibrium with the surrounding air only at supersaturations (Kelvin effect). Conversely, for $\Theta < 90°$, the curvature of the meniscus is negative and condensation can occur at subsaturation levels (Crouzet and Marlow, 1995). In the following, this phenomenon will be referred as inverse Kelvin effect. Already traces of adsorbates of only a fraction of a monolayer may significantly alter the wetability of the particle surface. Care has to be taken if these macroscopic phenomena are applied to microscopic particles.

In a recent paper (Weingartner *et al.*, 1995) the hygroscopic behavior of soot particles emitted from a four-stroke spark ignition engine (SI engine) using leaded fuel was investigated. It was found that water condenses on these combustion particles at subsaturations and that the hygroscopicity increases

‡ Author to whom correspondence should be addressed.

while the particles are aging. In this paper we attempt to quantify the hygroscopicity of soot particles emitted from a diesel engine combined with chemical and morphological analysis of the soot samples. In addition, the influence of the fuel sulfur content on the hygroscopicity is presented. Diesel engines are of great environmental concern because they are known to emit roughly about 100 times more fine particulate mass than SI engines.

2. EXPERIMENTAL

2.1. *Aerosol generation*

Two kinds of carbonaceous particles were investigated:

- Carbon particles produced by spark discharges between two graphite electrodes (Schwyn *et al.*, 1988) with nitrogen as carrier gas. These particles were highly agglomerated.
- Fresh combustion particles, emitted from a diesel engine (Yamaha EDA 4700 T, direct injection, no turbo charger) with 4 kW nominal electric output power. Measurements were performed at loads of 0, 1 and 2 kW, which corresponds to an air/fuel ratio λ of 5.8, 4.2 and 3.0, respectively (Steiner, 1993). The engine was run with commercially available diesel fuel (sulfur content $< 0.05\%$). In one part of the experiments 0.2 mass% sulfur (in form of di-tertiary-butyldisulfide) was added to the nearly sulfur free diesel fuel.

To prevent condensation of water, the sampled aerosol was immediately diluted with particle-free and dry air. Typical dilution ratios were about 1 : 50. Because the dilution air was heated to the exhaust gas temperature, the diluted particles never experienced an RH higher than 30%.

2.2. *Pre-treatment of the aerosol*

In some experiments, the aerosol particles were exposed to a defined ozone (O_3) concentration before entering the analyzing system. NO_x free O_3 was formed by irradiating particle free air with UV light (wavelength $\lambda = 172$ nm) emitted from an Xe_2-excimer lamp. More details about excimer UV sources are given by Kogelschatz (1992). The upper part of Fig. 1 illustrates that the O_3 was added to the aerosol and that behind the reaction vessel (with a residence time of 2 min) the O_3 was removed by an activated charcoal denuder. The O_3 concentration was monitored with a Dasibi 1003 AH ozone analyzer and was adjusted by the airflow through the excimer lamp (typically $0.1\,\ell\,m^{-1}$). Without addition of the exhaust gas, the O_3 concentration at the exit of the reaction chamber was lower (by about 25%) compared to the concentration at the vessel entrance. This is most probably due to wall losses in the chamber. A significant O_3 depletion caused by the diesel exhaust was also observed which is mainly explained by an oxidation of NO to NO_2. By mixing exhaust gas instead of pure air with a constant O_3 amount, the O_3 concentration decreased behind the reaction vessel from about 2 ppm to 0.1 ppm.

In other experiments the aerosol was pre-treated with UV light. This was performed by illuminating the aerosol with

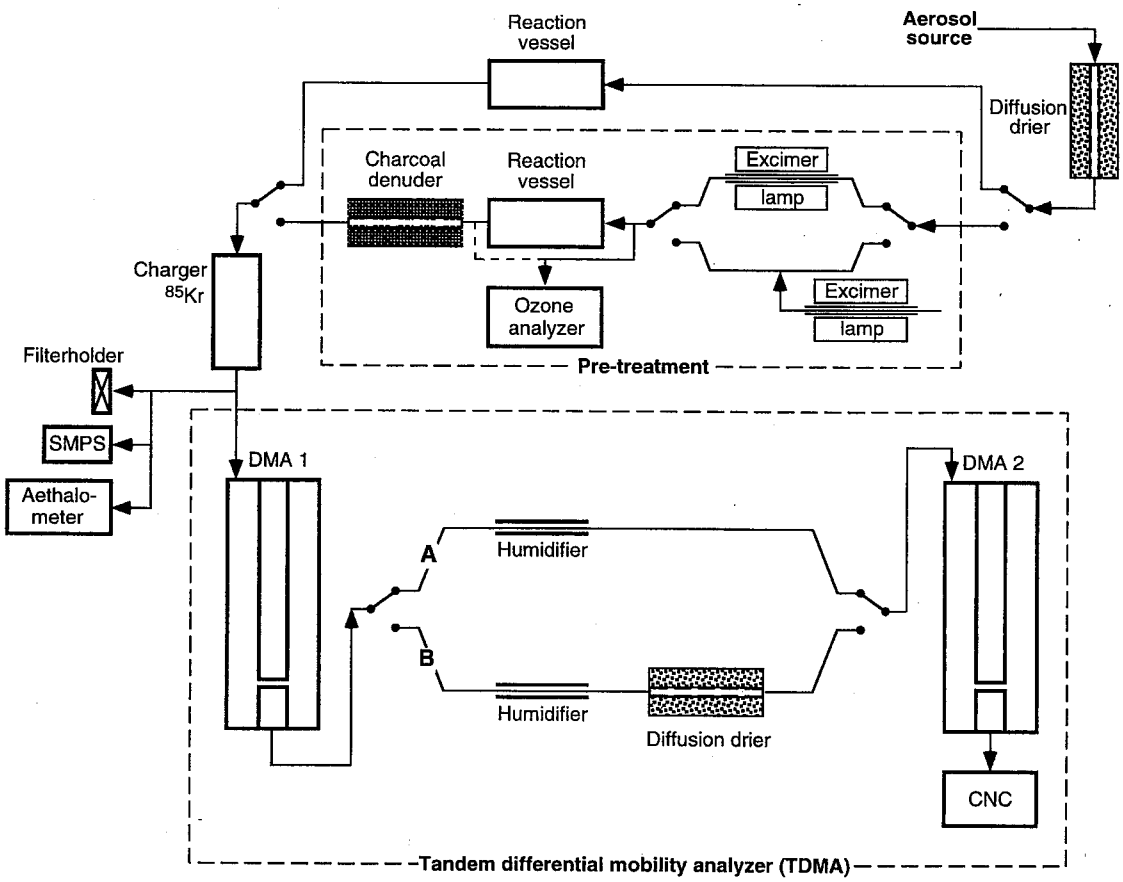

Fig. 1. Schematics of the experimental setup of the Tandem Differential Mobility Analyzer (TDMA). In position A the hygroscopicity and in position B restructuring of the particles is measured. In a part of the experiment the particles were pre-treated with ozone and UV radiation produced by an excimer lamp.

the same excimer radiation followed by a reaction vessel (residence time $t = 2$ min) and a charcoal denuder. Here, the O_3 concentration was adjusted by changing the intensity of the UV radiation.

2.3. *Measurement of the hygroscopicity*

A Tandem Differential Mobility Analyzer (TDMA) was used to measure the hygroscopic behavior of the combustion particles. The experimental setup of the TDMA used in this study is described in more detail in Weingartner *et al.* (1995). Briefly, Fig. 1 shows that before entering the TDMA, the aerosol was dried with a silicagel diffusion drier and then fed into a reaction vessel with a residence time of 2 min (RH $< 5\%$ at this point). After the first Differential Mobility Analyzer (DMA) the monodisperse aerosol was passed through one of two possible reaction processes. Thereafter, the size distribution was measured with a second DMA combined with a condensation nucleus counter (CNC). The sheath air of the second DMA was also humidified. The two different reaction processes between the two DMAs were:

Position A: Measurement of the hygroscopicity of the aerosol. The particles were humidified, and after 2.2 s at controlled RH, they entered the second DMA. To prevent a hysteresis effect in the particle growth, the RH in the second DMA was set 2% higher than the RH of the aerosol stream.

Position B: The restructuring of the aerosol was measured. Here, the aerosol was first humidified (during 2.2 s) and then dried in another diffusion drier with a residence time of about 10 s. The RH in the second DMA was set to be smaller than 5%.

Great care was taken to maintain constant temperatures and constant flows in the whole system. Therefore, the sheath air flows and excess air flows were controlled with mass flow controllers and critical orifices, respectively.

During a measurement, the humidities before and inside the second DMA were kept at a constant level. The first DMA voltage was kept fixed while the second was scanned to evaluate the changes of the electrical mobility diameter of the particles. The obtained size spectra were fitted with a Gauss function

$$C_i = A \exp\left(-\frac{1}{2} \frac{(U_i - U_m)^2}{\sigma^2} \right) \quad (1)$$

where A and σ are constants, C_i is the CNC count rate at the applied voltage U_i. The voltage with the highest count rate U_m was calculated by using the Levenberg–Marquardt algorithm (Press *et al.*, 1986). U_m is related to the mode diameter d_m (diameter with the highest count rate) (see Appendix equations (A4) and (A6)), which was used to calculate the growth factors d/d_0, defined as the ratio of the mobility diameter d of the humidified particles to the mobility diameter d_0 of the dry particles. The fitting procedure also calculated the confidence intervals assuming that the measured data points are normally distributed. In the figures the uncertainties of the growth factor are represented by vertical error bars. The RH was measured with a relative accuracy of $\pm 1.5\%$ (horizontal error bars). Since the observed growth factors showed no significant size dependence, it was not necessary to apply a correction for doubly charged particles.

In our setup the relation between the applied voltage (on the center electrode of the DMA) and the mobility diameter is weakly dependent on RH. If the experiment was run under position A, this effect was considered with the following empirical correction (for details see Appendix):

$$d_p^{real}/d_p^{measued} = 1 - c\mathrm{RH}[\%] \text{ with}$$
$$c = 6.5 \times 10^{-5} \pm 0.3 \times 10^{-5} \quad (2)$$

where d_p^{real} denotes the real mobility diameter calculated with consideration of the actual RH and $d_p^{measured}$ the mobility diameter calculated for dry air.

2.4. *Measurement of the morphology and chemical composition of the particles*

Samples for the morphological and chemical analysis were taken at the TDMA entrance and the polydisperse particles experienced the same history (i.e. same dilution ratio, residence times, gas temperatures) as in the hygroscopicity experiments.

For determination of the morphology of the particles, microscopy samples were collected at the TDMA entrance on silver filters with a pore size of 450 nm (Millipore, AG4502500). Microscopy was performed with a High Resolution Scanning Electron Microscope (HRSEM, Hitachi S-900, in-lens field emission SEM, Nagatani *et al.*, 1987) operating at a primary acceleration voltage of 30 kV and a beam current of 10^{-11} A. Cryotechniques could be applied in order to prevent desorption of semi-volatile material (e.g. the samples were frozen in liquid nitrogen and mounted on a Gatan cryo-holder and cryo-transferred into the SEM where they were observed at temperatures down to -160°C). Seven filters with diesel engine particles and two filters with carbon particles were analyzed (with and without cryotechniques), and photographs of more than 100 particles were taken.

Samples for chemical analysis were taken on quartz fiber filters. Diesel engine particles produced with sulfur enhanced fuel at 0 and 1 kW load were sampled. Furthermore, samples were taken from the SI engine. The hygroscopic behavior of these gasoline particles is described elsewhere (Weingartner *et al.*, 1995). The exposed parts of the filters were cut out and the soluble fraction of the soot was ultrasonically extracted in 3 ml deionized water during 45 min at 30°C. Ion chromatography (IC, mixed Sykam/Dionex system) was performed for a quantitative determination of anions. The black carbon (BC) content of the filters was determined with an aethalometer (AE9, Magee Scientific, Hansen *et al.*, 1984) by assuming an absorption coefficient of $\sigma = 19\ \mathrm{m^2\,g^{-1}}$. For the diesel particles, an SMPS (differential mobility analyzer (DMA) combined with a condensation nucleus counter (CNC)) continuously monitored the particle size spectrum. This allowed calculation of the total equivalent surface (i.e. surface of spheres with the same mobility diameter distribution) of the particles deposited on the filters.

3. RESULTS AND DISCUSSION

3.1. *Morphology*

Particles with diameters in the size range between 20 and 500 nm were examined by high-resolution scanning electron microscopy. Figure 2 shows typical micrographs of sampled carbon and diesel particles.

Figures 2A(1–3) show carbon particles in their original state. The samples were transported and prepared in a dry atmosphere. These carbon particles are agglomerates with an irregular structure forming branched chains. The primary particle diameter is found to be about 10 nm. The fractal-like dimension of these particles was investigated *in situ* with a DMA combined with a low-pressure impactor (Schleicher *et al.*, 1995) and was found to be $D_f = 2.10$ (Weingartner *et al.*, 1995). Because the carbon particles are only formed by aggregation (and not by coalescence or condensation of volatile material), this value can be compared with the results predicted by computer

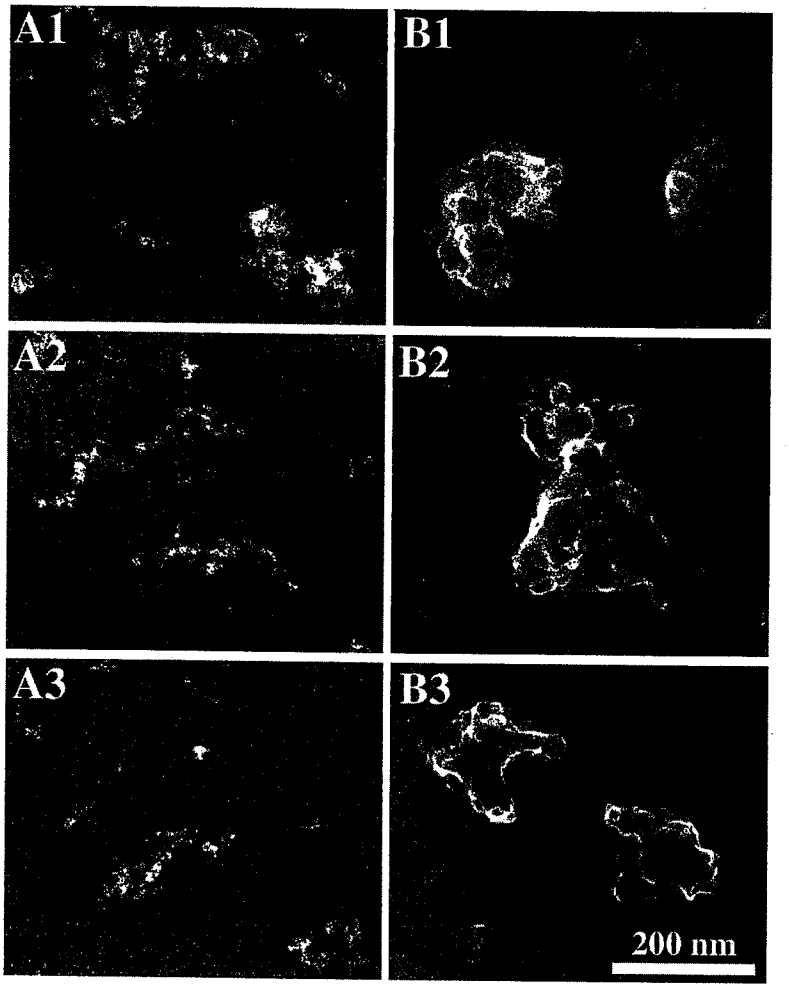

Fig. 2. Secondary electron images obtained with a High Resolution Scanning Electron Microscope (HRSEM) of carbon particles (A1, A2 and A3) and particles emitted from the diesel engine at 1 kW load with sulfur enhanced fuel (B1, B2 and B3). A1 and B1 were observed at ambient temperature (21°C) whereas A2, A3, B2 and B3 were observed at − 95°C. The scale bar applies to all pictures.

simulations for cluster–cluster aggregation, which typically give a D_f between 1.8 and 2.0 (Jullien *et al.*, 1987).

Figures 2B(1–3) show particles emitted from the diesel engine operated at 1 kW load. The mean diameter of the primary particles was found to be about 25 nm. In contrast to the carbon particles, the diesel particles exhibit a more compact structure with less visible primary particles. Particles produced in idling motion showed a similar compact structure. The morphological shape of the diesel particles did not change significantly when they were observed without cryotechniques, or when the samples were coated with a 1 nm thick tungsten layer. The compact morphology of these particles is supported by fractal analysis: First measurements with a DMA combined with a low pressure impactor gave a D_f close to 3 for particles with $50 < d < 150$ nm (Skillas, 1996, personal communication). Similar high fractal dimensions were also measured on particles emitted from the SI engine (Burtscher *et al.*, 1995).

The compact structure as well as the high values of D_f found in this study for the diesel particles differ from the findings reported in other studies. This is most probably due to different size ranges that were analyzed, as well as due to different measurement methods. Weber *et al.* (1996) found two different values for D_f of silver agglomerates as a function of size, with $D_f \approx 3$ below a critical diameter. They related this observation to two different coagulation regimes depending on the ratio of the agglomerate diameter to the mean free path of the primary particle. In addition, it may be expected that for small combustion particles D_f is increased by embedding of the primary particles with hydrocarbons, e.g. lubricating oil, unburned fuel and polycyclic aromatic hydrocarbons (PAH) (Needham *et al.*, 1989). Therefore, lower values of D_f are expected at larger agglomerate

diameters also for combustion particles, however, they were not accessible with the present system.

Lower fractal dimensions were also found using transmission electron microscopy (TEM) images. Nelson *et al.* (1990) report a two-dimensional D_f between 1.5 and 1.8 for diesel particles with diameters of about 600 nm. In our study, SEM pictures were obtained using the secondary electron signal (note that the particles of Fig. 2 were not coated with conducting material). The detected secondary electron origin from the very surface of the sample (up to a depth of about 1 nm), and therefore give a surface image, in contrast to TEM pictures, where the image is formed by the mass density dependent bright field signal. To our knowledge, no systematic study has been performed so far on the differences of D_f obtained from TEM and SEM pictures.

3.2. *Chemical composition*

The results of the chemical analysis for particles emitted from the SI and diesel engine are listed in Table 1. The SI engine was operated with leaded fuel (0.15 g Pb/l) and the diesel engine with the sulfur enhanced fuel. Several filters were analyzed and the mean values with their standard deviations are shown. The values were corrected for the ion concentrations found on blank filters. These filters were subjected to the same exhaust gas volume where the particles were already removed by another filter. To compare the chemical composition of the particles emitted from the two engines, the masses of the individual ions were normalized to the BC mass content of the particles. The NO_2^- and NO_3^- ion concentrations showed a large scattering. Therefore, only an upper limit of these values is presented. This high variability is most probably caused by the fact that the adsorption of NO_x is highly sensitive on the chemical situation of the substrate. In addition, it cannot be excluded that adsorption and subsequent oxidation takes place on the quartz filter material or on exhaust gases adsorbed to the quartz fibers. This hypothesis is corroborated by high blank values of the filters treated with filtered exhaust gas. In the following, the NO_2^- and NO_3^- data are therefore not considered. A comparison between the two engines shows that much higher ion to BC ratios were found for the SI engine particles. The high Cl^- and Br^- contents of the SI engine particles are due to the use of ethylene dichloride and ethylene dibromide as additives in the leaded gasoline fuel. Differences were also reported for the organic fraction. Steiner *et al.* (1992) measured the BC content of the particles emitted from the same SI engine operating with leaded fuel at medium load and found that only 2.5% of the total particulate mass was BC. In contrast, the BC fraction of the diesel engine particles was considerably higher (about 80%, 40% and 28% at 2, 1 and 0 kW load, respectively, Burtscher *et al.*, 1993). The detailed mechanisms responsible for the concentrations of the ions as well as of the organic fraction are complex. It can be expected that the engine type, the air/fuel ratio, the combustion temperatures as well as the type of fuel play an important role.

Table 1. The results of the chemical analysis of particles emitted from the SI engine and the diesel engine. The ratios of the ion mass to the BC mass as well as the ion surface dencity ρ_i are given

	SI engine	Diesel 1 kW	Diesel 0 kW
	Ion to BC ratio		
Br^-	12.5 ± 5.8	n.d.	n.d.
Pb^{2+}	41.2 ± 11.8	n.d.	n.d.
Cl^-	2.35 ± 1.03	0.0041 ± 0.0037	0.0070 ± 0.0066
NO_2^-	< 0.08	< 0.14	< 0.33
NO_3^-	0.06 ± 0.05	< 0.043	< 0.09
SO_4^{2-}	0.29 ± 0.06	0.031 ± 0.014	0.035 ± 0.007
	ρ_i (nm^{-2})		
Cl^-	n.d.	1.0 ± 0.9	1.9 ± 1.8
NO_2^-	n.d.	< 32	< 68
NO_3^-	n.d.	< 6	< 14
SO_4^{2-}	n.d.	2.8 ± 1.2	3.5 ± 0.7

n.d.: not detected

Specific surface ion densities ρ_i for each component were calculated with the SMPS data (see Table 1). ρ_i was calculated by dividing the amount of ions of a specific type (determined with the chemical analysis) by the total particle surface area (calculated from the SMPS). For the Cl^- and SO_4^{2-} ions surface ion densities ρ_i between 1 and 3.5 nm^{-2} were found.

3.3. *Hygroscopic behavior of carbon particles*

In Fig. 3a measurements with carbon particles produced by spark discharges between two graphite electrodes are shown. The carrier gas was nitrogen with a purity of 99.999% and the TDMA was operated in position A. Figure 3a shows that these particles shrink with increasing RH. The data were fitted with regression lines $d/d_0 = a\,\mathrm{RH}(\%) + 1$. In Fig. 3b the slope a, which is a measure for the shrinking of the particles, is plotted versus the dry particle diameter d_0. It can be seen that the shrinking starts at a diameter d_0 of about 15 nm and is more pronounced for larger particles. This value agrees very well with the primary particle diameter of about 10 nm determined from the HRSEM pictures. From $d_0 = 15$ nm to $d_0 = 50$ nm the shrinking of the particles increases linearly and changes its slope for $d_0 > 50$ nm. Measurements were also performed with the TDMA operating in position B. Within the accuracy of the measurement the same shrinking factors were obtained, which indicates that the restructuration is an irreversible process.

The observed shrinking is explained with a restructuring of the agglomerated particles. In a previous paper (Weingartner *et al.*, 1995) the fractal dimension D_f of the carbon particles was investigated before and after an exposure to RH = 90% and it was found that D_f increased from 2.10 to 2.17. Due to the inverse

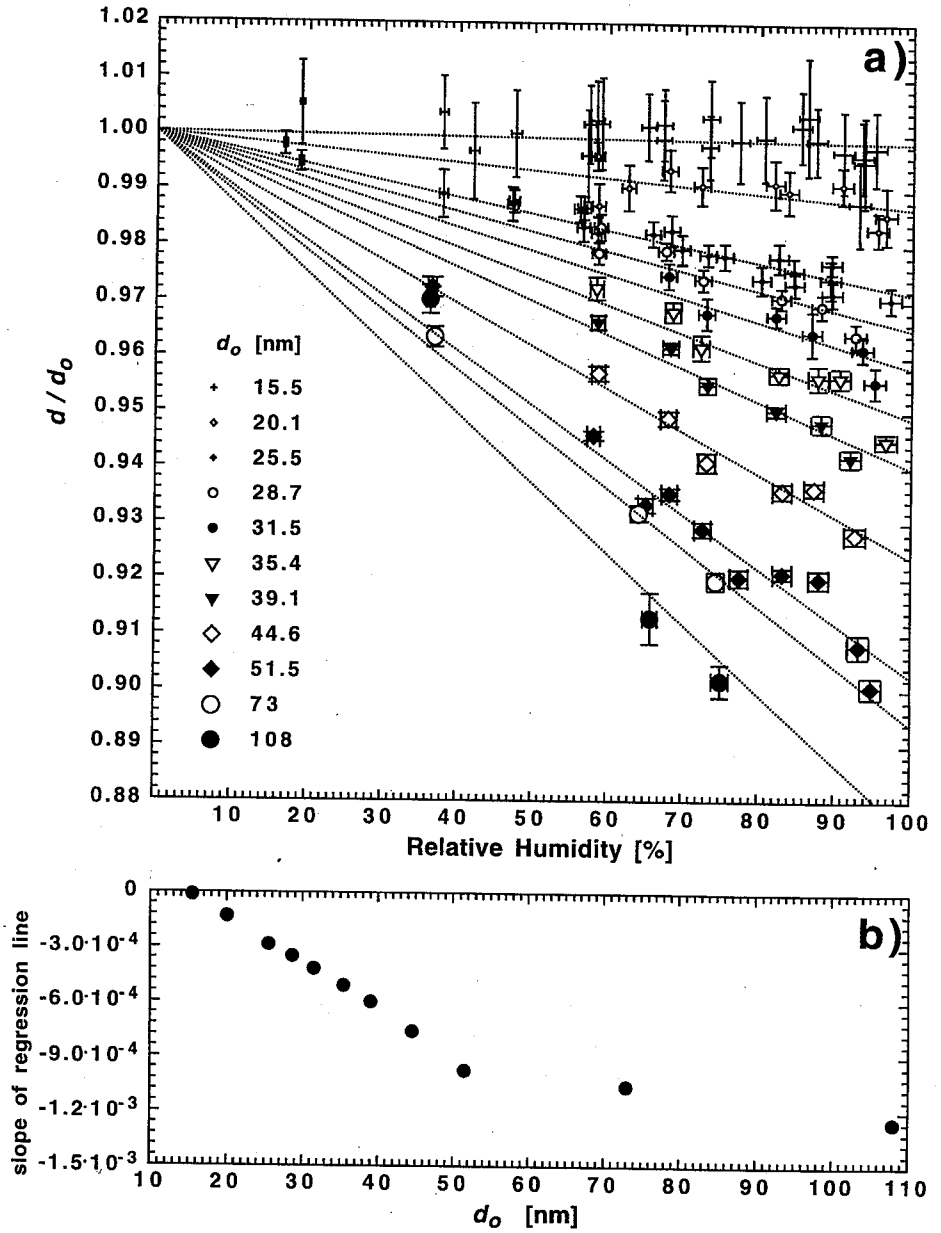

Fig. 3. (a) Growth factor d/d_0 vs. relative humidity for carbon particles for different dry diameters d_0. $d/d_0 < 1$ indicates a restructuring of the particles. The data with d_0 = constant were fitted with regression lines. In (b) the slopes of these regression lines vs. the diameters d_0 are shown.

Kelvin effect water condenses in small angle cavities of the particles. This leads to capillary forces on the branches of the aggregates, causing them to collapse. One can imagine that the wetability of the surface is enhanced by polar carbon–oxygen and carbon–nitrogen groups. Weller and Young (1948) stated that adsorption of water on carbon is increased by a treatment of the carbon with oxygen. Fendel *et al.* (1995) showed that carbon particles with an initial diameter of 7 nm adsorb more than one monolayer of O_3 at concentrations higher than 40 ppb. Therefore, experiments were performed by exposing the carbon particles to a fixed O_3 concentration. However, we did not observe a significant change in the restructuring behavior of carbon particles with 50 nm $< d_0 <$ 110 nm after exposing them to an O_3 concentration of 3 ppm during 2 min. Therefore, it can be hypothesized that the O_3 treatment did not significantly change the wetability of the particle surface.

3.4. *Hygroscopic behavior of diesel engine particles produced under load*

Figure 4 shows the change of the mobility diameter as a function of RH for freshly emitted diesel engine

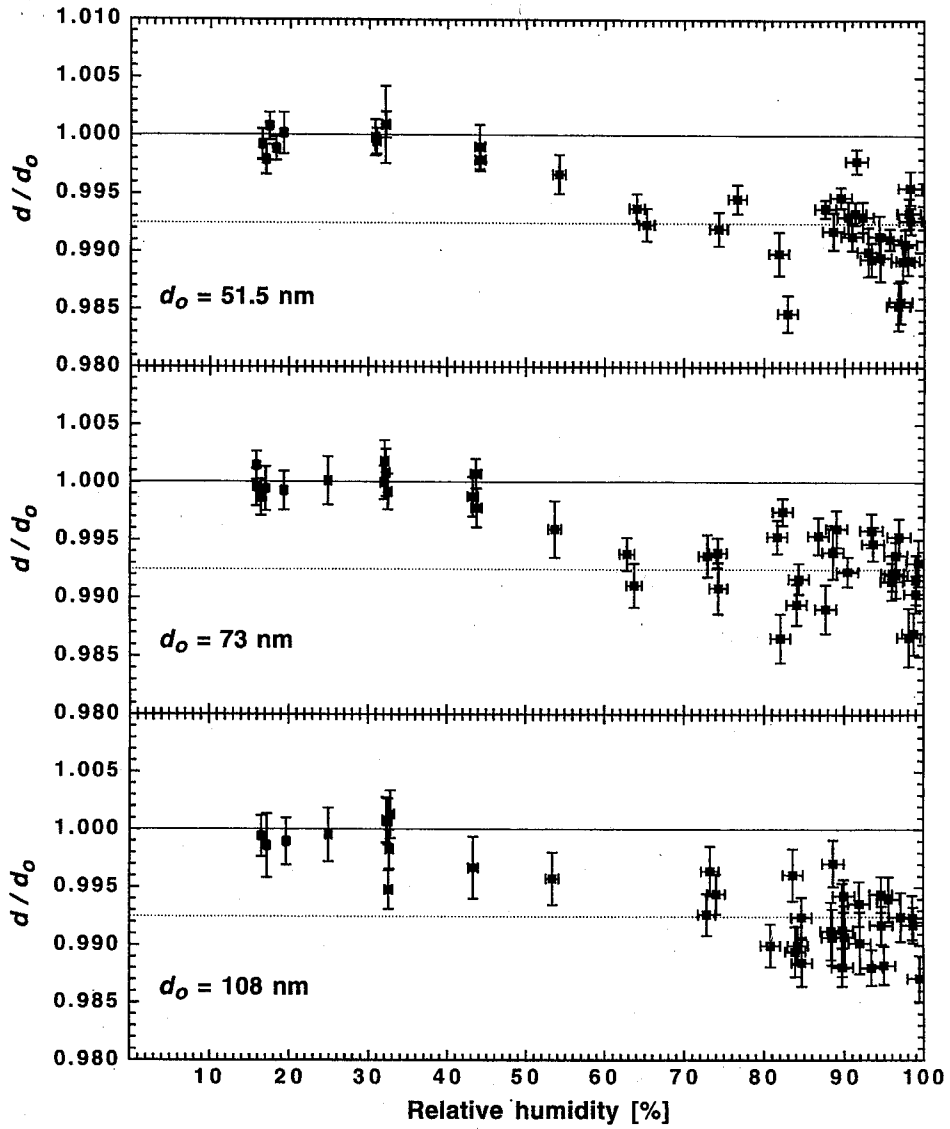

Fig. 4. The restructuring of diesel engine particles (1 kW load, no fuel additives) with dry diameters of $d_0 = 51.5$, 73, and 108 nm. These measurements were performed with the TDMA operating in position B.

particles. Particles with $d_0 = 51.5$, 73 and 108 nm were investigated. The TDMA was operated in position B, i.e. the dry, monodisperse particles were exposed to higher RH and then dried again. The diesel engine was operated at 1 kW load without fuel additives. It is seen that these particles start to shrink at about RH = 40% and reach a growth factor of $d/d_0 \approx 0.9925$ at RH > 65%.

Evidently, the diesel particles undergo less restructuration than the carbon particles. The main reason for this difference is most probably the different morphologies of the particles: As seen in the HRSEM pictures, the diesel particles are more compact and they show less branched chains than the carbon particles. Therefore, they have a smaller restructuring ability. The cavities of diesel particles (e.g. between contacting primary spheres) are filled to some extent with semi-volatile material. These adsorbates may increase the binding between the primary particles and they may also lower the restructuring ability. Furthermore, these volatile compounds (which have condensed onto the aggregates during the cooling of the exhaust gas) might also have induced capillary forces and lead to a restructuring of the particles. Moreover, if adsorbed material is present on an aggregated particle, it is possible that the negative curvature of these capillaries is less distinct. For a given RH less water condenses in the "smoother" capillaries leading to a smaller restructuration.

Until now, little is known about surface wetting properties of carbon and diesel particles, mainly because wetability strongly depends on the chemical

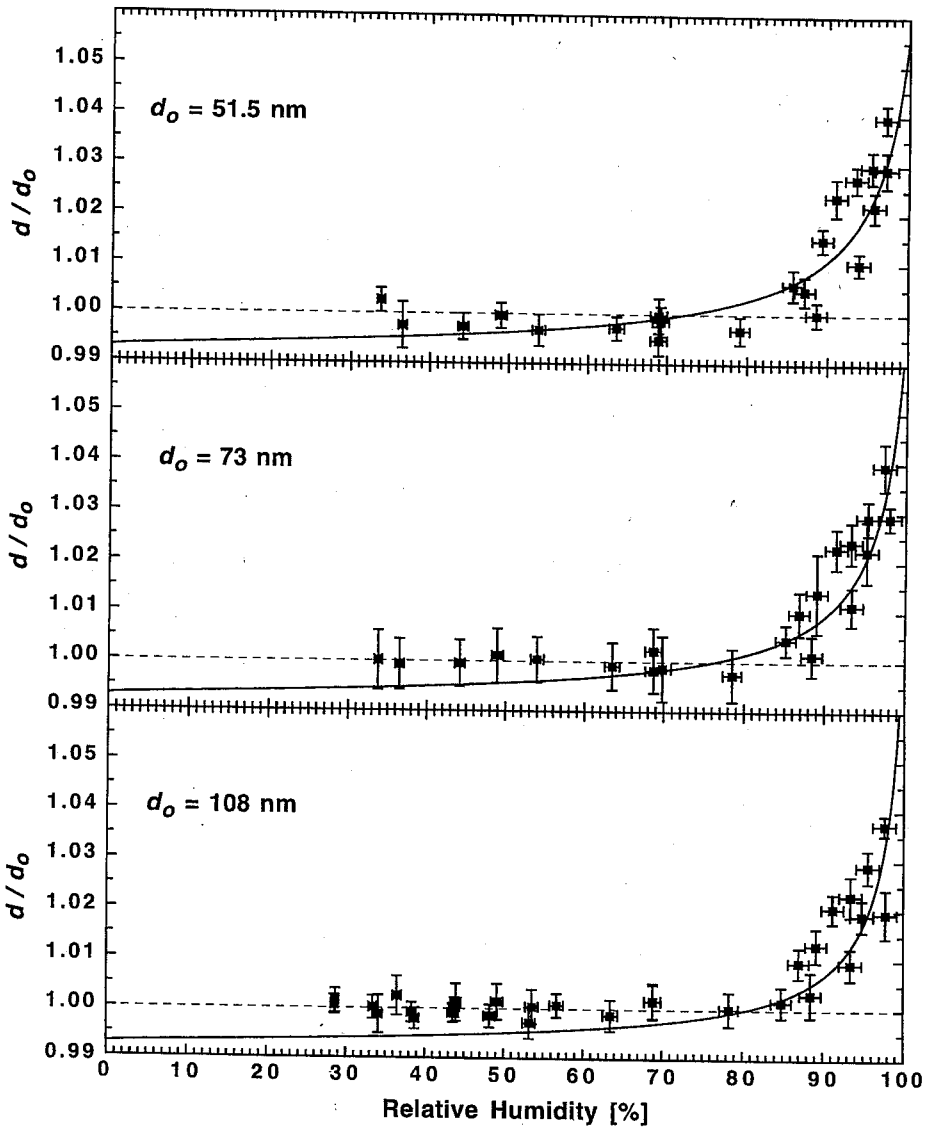

Fig. 5. Hygroscopic growth of particles emitted from the diesel engine operating at 1 kW load (no fuel additives, no pre-treatment of the aerosol). The TDMA was operated in position A. The solid lines are fitted Köhler curves (see text).

composition and the micro-structure of the particle surface.

In Fig. 5 the hygroscopic growth of the same diesel particles (engine load 1 kW, no fuel additives and no pre-treatment) was investigated by using TDMA position A. It can be seen that these combustion particles start to grow at about 80% RH and reach a growth factor of about $d/d_0 = 1.025$ at RH = 95%.

To classify the data, the points were fitted with modified Köhler curves. The Köhler model relates the diameter d of a droplet (containing dissolved materials and a water insoluble core, diameter d_0) with the water vapor pressure e_r on its surface. The saturation ratio $S = \mathrm{RH}/100\% = e_r/e_{sat,w}$ over a sufficiently diluted solution is given by (Pruppacher and Klett, 1980):

$$S = \exp\left[\frac{4M_w\sigma}{RT\rho_w d}\right]\exp\left[-\frac{6\ \nu m_s M_w}{\pi\ (d^3 - d_0^3)\ M_s\ \rho_w}\right]. \quad (3)$$

$e_{sat,w}$ is the water vapor pressure over a plane surface, M_w the molecular weight of water, σ the surface tension of pure water, R the gas constant, T the temperature, ρ_w the density of water, ν the number of ions each molecule forms when it dissolves and m_s the mass of the solvent having a molecular weight M_s. The first term considers that e_r over the drop surface is enhanced by a curvature effect (Kelvin effect), and the second term is the Raoult's law, which describes the decrease of the water vapor pressure by the

solute material. For $T = 293$ K equation (3) can be simplified to

$$S = \exp\left[\frac{\alpha}{d}\right] \exp\left[-\frac{\beta N_I}{(d^3 - d_0^3)}\right] \quad (4)$$

with $\alpha = 2.155$ nm and $\beta = 5.712 \times 10^{-2}$ nm^3. N_I denotes the amount of dissociated molecules in the water layer of the droplet. This model is not strictly applicable to combustion particles because it assumes that the droplets – as well as the insoluble core – are spheres. Furthermore, it assumes that the vapor pressure is reduced only according to Raoult's law. Shulman *et al.* (1996) recently showed that σ is lowered by dissociated compounds. This leads to an additional reduction of the vapor pressure and thus to a further decrease of the critical supersaturation. Nevertheless, this semi-empirical model is a useful tool to obtain an estimate of the amount of dissociated molecules N_I in the water layer. These molecules are responsible for a reduction of the vapor pressure at the particle surface. The amount of N_I will determine to what extent the particle will grow by water condensation. In Fig. 5 and the following figures the data were fitted by equation (4). The Köhler curves are based on the assumption that during the growth of the diesel particles the insoluble core undergoes the same degree of restructuration as observed in Fig. 4. In other words, we assume that diesel particles with $50 < d_0 < 110$ nm start their hygroscopic growth at a diameter $d^* = 0.9925\ d_0$. Only points with RH $> 80\%$ were used for the fit. This was done because the points with RH $< 80\%$ have a large weight on the fitted curve and the restructuration process has not reached its steady state at RH $< 80\%$ (see Fig. 4).

Figure 6 shows measurements performed under the same conditions as in Fig. 5 (1 kW load, TDMA position A), but with enrichment of the diesel fuel with 0.2 mass% sulfur. It is clearly seen that the hygroscopic growth of these particles is more pronounced compared to the measurements without fuel additives (Fig. 5), which is reflected in higher values of N_I. Measurements performed at 2 kW load with the sulfur enhanced fuel showed a similar growth behavior as at 1 kW but with higher N_I for larger particles. N_I was increased by about 5, 70, and 60% for $d_0 = 51.5$, 73, and 108 nm, respectively. The obtained values of N_I are summarized in Table 2. The indicated errors were determined by variation of N_I such that all measured data with RH $> 80\%$ were within the error range.

In a recent paper (Weingartner *et al.*, 1995) measurements of the hygroscopicity of freshly emitted particles from an SI engine using leaded fuel were presented. The observed hygroscopic growth was compared with Köhler curves (calculated with equation (4)) and N_I was estimated. Because the degree of restructuration was not determined, only a raw estimate of N_I can be given. We assume that before the particles start their hygroscopic growth they experience a restructuration of $d/d_0 = 0.996$, 0.99, and 0.985 for $d_0 = 51.5$, 73, and 108 nm, respectively. These values are estimates based on the measured growth curves. N_I was found to be 10000 ± 8000, $20{,}000 \pm 15{,}000$, and $120{,}000 \pm 80{,}000$ for $d_0 = 51.5$, 73 and 108 nm, respectively. It is obvious—despite the uncertainties—that the gasoline particles have a smaller hygroscopic growth than the diesel particles measured under load.

From the fitted parameter N_I, obtained for diesel engine particles, equivalent surface densities $\rho_s = N_I/A$ of the dissolved molecules were calculated, where A is the surface of a sphere with diameter d_0. Values between 2 and 10 nm^{-2} were obtained (see Table 2). ρ_s shows a smaller size dependence than N_I with higher densities for larger particles. For comparison, a monolayer of NaCl (with a thickness of 0.3 nm and a density of 2.17 g cm^{-3}) would have an ion surface density of $\rho_s = 13.4$ nm^{-2} on a spherical particle surface. Anyhow, we do not know how the soluble material is distributed over the particle surface. For the measurements performed at an engine load of 1 kW with sulfur enhanced fuel the values of ρ_s can directly be compared with the specific surface ion densities ρ_i obtained for the same particles by chemical analysis (see Table 1). It can be seen that the applied Köhler model predicts a total ion surface density that is of the same order of magnitude as the measured values, if the NO_2^- and NO_3^- data are neglected. However, it must be kept in mind that the chemical analysis did not measure all ions and soluble compounds. In addition, it is not known if during our experiment all soluble compounds in the aerosol particle were dissolved. One can imagine that ions that are embedded in the adsorbed material do not dissolve during the exposure of 2.2 s to RH. It can be expected that particles subjected to a longer exposure to RH will manifest a higher hygroscopicity. However, the influence of the duration of the RH exposure on the particles hygroscopicity needs to be investigated in further experiments.

3.5. *Hygroscopic behavior of particles from the idling diesel engine*

A completely different hygroscopic behavior was observed for particles produced by the idling diesel engine (see Fig. 7). These particles were also measured in TDMA position A. In contrast to the measurement at 1 kW load, no hygroscopic growth at higher RH was observed. The particles produced without fuel additives shrank with increasing RH to a growth factor d/d_0 of about 0.99 at RH = 90%. An even higher shrinking of particles produced with sulfur enhanced fuel was observed ($d/d_0 \approx 0.96$ at RH = 90%). The lack of a hygroscopic growth is in contradiction to the relatively high ion surface densities found for these particles (see Table 1). We suppose that this difference is due to the high organic fraction of particles emitted from the idling diesel engine. Bäcker (1991) reported that with increasing air/fuel

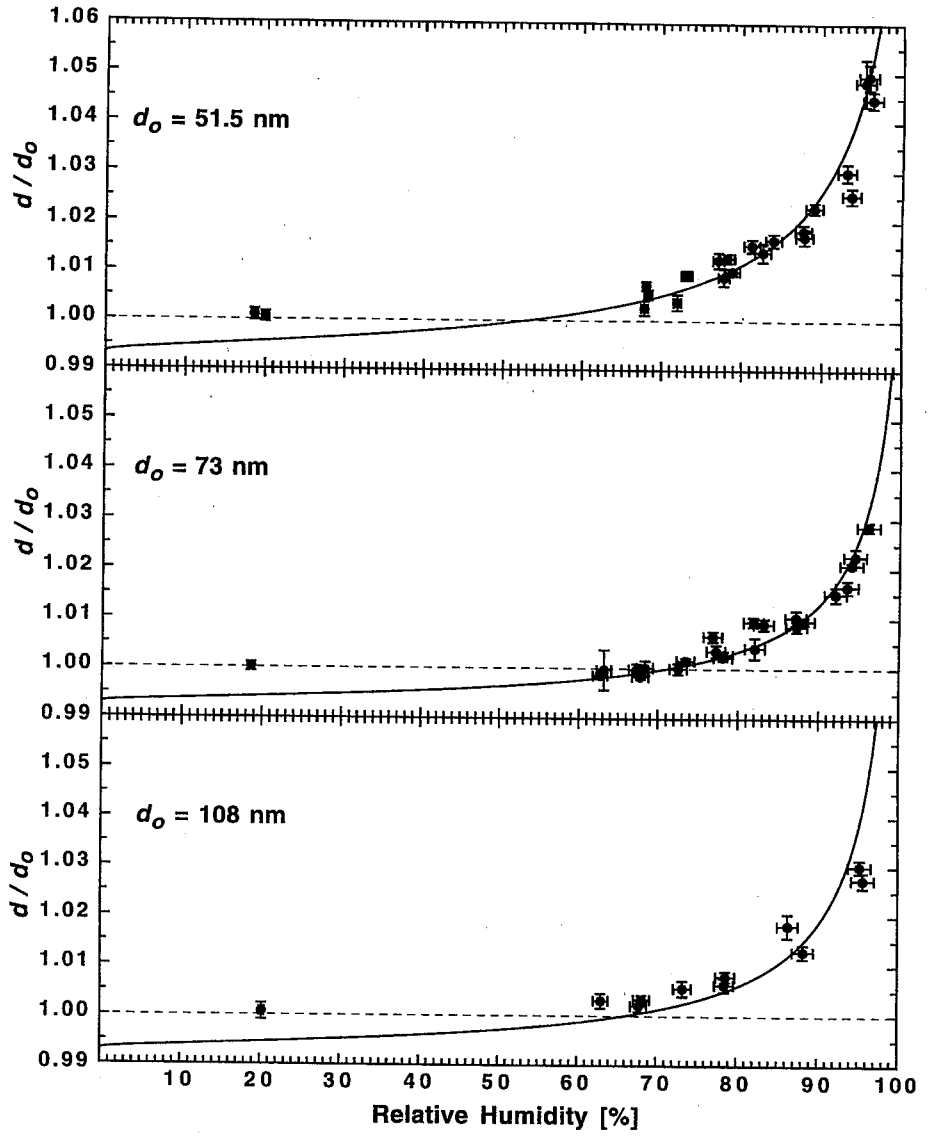

Fig. 6. Hygroscopic growth of particles emitted from the diesel engine operating at 2 kW load (sulfur enhanced fuel, no pre-treatment of the aerosol) and the fitted Köhler curves. The TDMA was operated in position A.

ratio λ (i.e. decreasing engine load) the fraction of paraffins (C_{15}–C_{30}) on diesel engine particles increased. These species are adsorbed on the particles and may impede the transfer of water across the surfactant layer of the particle. This organic barrier prevents material to dissolve, i.e. a growth of the particles by water condensation is hindered, as also shown by Saxena *et al.* (1995) and Dua and Hopke (1996).

A possible hypothesis for the observed distinct restructuration is that as a result of the incomplete combustion carboxylic acids, carboxylates and sulfonic acids are expected to be present in the organic fraction. One end of such molecules is water attractive and the other is water repelling. These molecules may exhibit a soaplike surfactant behavior and thus could be responsible for the particle surface to become more hydrophilic. However, if they are not water soluble they would not contribute to a hygroscopic growth.

3.6. *Pre-treatments with* O_3 *and UV radiation*

The results of measurements with pre-treated diesel exhaust are included in Table 2. In a first part of these experiments, the exhaust gas of the diesel engine operating without fuel additives and at 1 kW load was pre-treated with O_3. Before entering the TDMA the polydisperse aerosol was mixed with 0.4 ppm O_3 and was allowed to react during 2 min before ozone was removed by an activated charcoal denuder. We observed an increased hygroscopic growth expressed in higher N_I. Compared to the values obtained without pre-treatment, N_I was enhanced by about 46, 24, and

Table 2. Determined amount of dissociated molecules N_I per particle with a dry diameter d_0 for different diesel engine loads, aerosol pre-treatments and sulfur content in the diesel fuel. n is the number of measurements which were used to calculate N_I. ρ_s is the calculated surface density of the dissolved molecules on an equivalent particle surface. d_c is the critical diameter and S_c is the corresponding critical supersaturation predicted by the Köhler model

Sulfur content of diesel fuel		< 0.05%	< 0.05%	< 0.05%	0.20%	0.20%
Pre-treatment to the aerosol		None	400 ppb O_3 no UV	400 ppb O_3 with UV	None	None
Engine load (kW)		1	1	1	1	2
	Dry diameter d_0 (nm)					
	51.5	11	5	9	11	10
n	73	11	5	9	11	8
	108	11	5	9	4	8
	51.5	18,000 (− 4000/ + 8000)	24,200 (− 4000/ + 1000)	26,200 ± 4000	33,100 ± 4000	35,000 (− 6000/ + 8000)
N_I	73	49,900 (− 15000/ + 30000)	57,100 (− 20000/ + 7000)	61,700 ± 10000	60,900 (− 10000/ + 20000)	104,300 (− 20000/ + 40000)
	108	118,100 (− 40000/ + 60000)	175,400 (− 60000/ + 40000)	143,500 ± 40000	216,200 (− 40000/ + 120000)	346,600 (− 80000/ + 100000)
	51.5	2.16	2.90	3.14	3.97	4.20
ρ_s (nm^{-2})	73	2.98	3.41	3.69	3.64	6.23
	108	3.22	4.79	3.92	5.90	9.46
	51.5	66.0	69.3	70.4	73.8	74.7
d_c (nm)	73	102.4	104.9	106.5	106.2	119.9
	108	151.0	164.0	157.0	172.6	197.7
	51.5	2.68	2.48	2.43	2.27	2.23
S_c (%)	73	1.69	1.63	1.59	1.60	1.35
	108	1.13	1.00	1.07	0.94	0.79

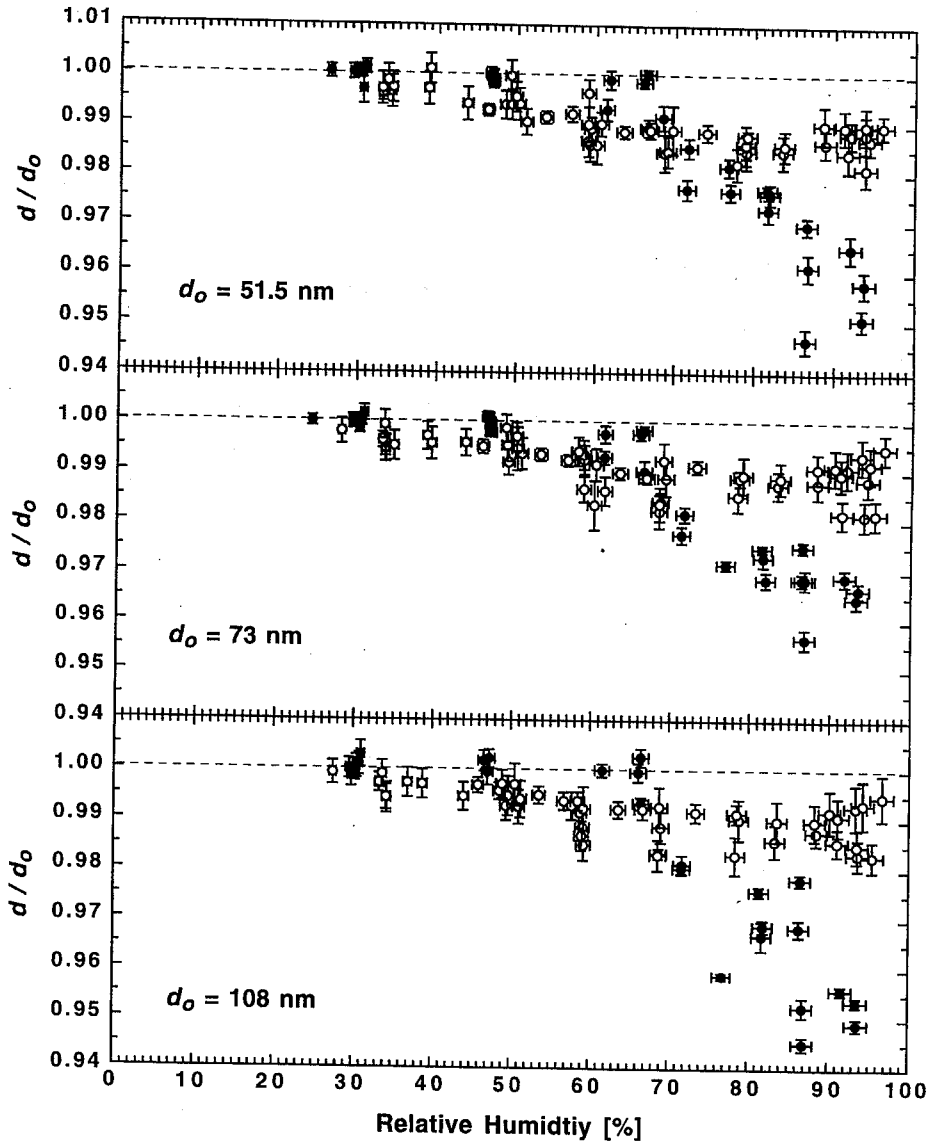

Fig. 7. Growth factor d/d_0 vs relative humidity for particles emitted from the diesel engine in idling motion. Measurements with no fuel additives (o) and with sulfur enhanced fuel (●) are shown. The TDMA was operated in position A.

22% for d_0 = 51.5, 73, and 108 nm, respectively. The hygroscopicity seemed to be further enhanced when the aerosol was subjected to UV radiation during 0.11 s. The intensity of the radiation was adjusted so that the produced O_3 was 0.4 ppm. As in the previous experiment the aerosol particles were allowed to react with the O_3 (and other photochemically produced products) during 2 min. Compared to the experiment where the exhaust gas was simply ozonated, N_1 was enhanced for d_0 = 51.5 and 73 nm but lowered for d_0 = 108 nm. However, because of the large scatter of the data these differences are not significant. Additional measurements were performed with the same set-up but with the excimer lamp being switched off. In this case we did not observe a change of the particle hygroscopicity, indicating that there was no artefact by the activated charcoal denuder.

The increased hygroscopicity in the case of the O_3 pre-treatment can be explained by a chemical modification of the particle surface. Matter *et al.* (1995) showed that O_3 adsorbs on diesel soot particles, which leads to a degradation of particle bound PAH. Therefore, it is possible that O_3 oxidizes the adsorbed hydrocarbons leading to more polar compounds, such as alcohols (R-OH), carboxylates (R-COOH), Oxo-PAH, and enhances the solubility of these particles (Chughtai *et al.*, 1991).

If the particles are irradiated additionally with UV light, they become more hygroscopic by, e.g., PAH photolysis (Kamens *et al.*, 1988). An oxidation of the

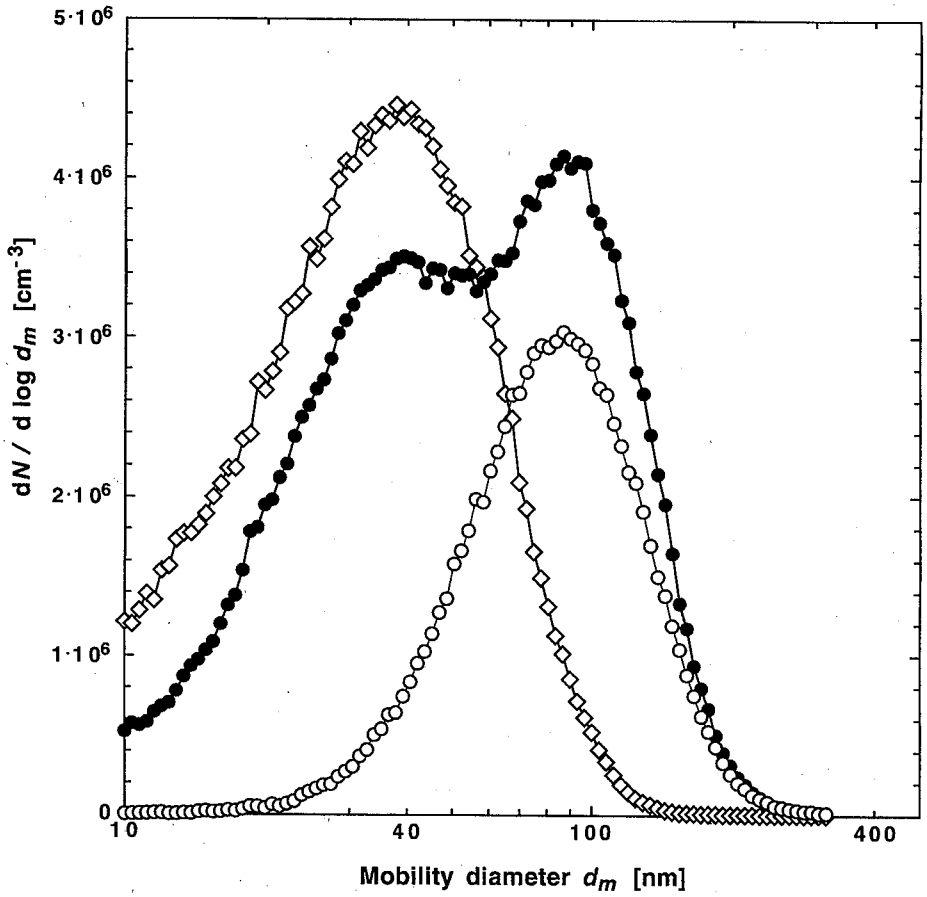

Fig. 8. Size spectra of diesel engine particles (1 kW load, no fuel additives) without pre-treatment (○) and after an exposure of the aerosol to 37 ppm O_3 (●). If the particles are removed with a filter and only the gas phase is subjected to the same pre-treatment, then particles produced by homogeneous nucleation appear at a mode diameter of about 40 nm (◇). Due to variations in the dilution ratio an absolute comparison of total number concentration is difficult.

particle surface from photochemically produced hydroxyl radicals (OH) is another possibility that needs to be investigated. Moreover, heterogeneous nucleation of photochemically produced species cannot be excluded. Size spectra of the pre-treated aerosol were measured behind the charcoal denuder with an SMPS. At O_3 concentrations of 0.4 ppm the size spectra did not significantly change compared to spectra of the untreated aerosol. At higher O_3 concentrations (typically > 4 ppm) the formation of new particles with $d < 100$ nm was observed. As an example, Fig. 8 shows size spectra of diesel engine particles (1 kW load, no fuel additives) with and without UV and O_3 pre-treatment. After an exposure to UV radiation and 37 ppm O_3 a bimodal distribution was measured, i.e. new particles were produced by homogenous nucleation. UV radiation initiates a chain of gas-phase reactions in the exhaust gas leading to condensation of condensable vapors (photochemical smog). If the soot particles were removed by a filter and only the gas phase of the exhaust gas was subjected to the UV and O_3 treatment, the nucleated particles appeared at a mode diameter of about 40 nm. Particles with $d_0 = 73$ nm that experienced higher O_3 concentrations showed a significantly enhanced hygroscopicity at RH = 95% ($d/d_0 \approx 1.05$ at 8 ppm O_3 and $d/d_0 > 1.1$ at 37 ppm O_3). We cannot exclude that at an UV pre-treatment with an O_3 concentration of 0.4 ppm a small amount of photochemically produced species condense onto the soot particles leading to an increase of the hygroscopicity of these particles.

3.7. *Calculation of critical supersaturations*

From the fitted parameter N_1 the critical diameter d_c as well as the critical supersaturation S_c required to activate a particle to a cloud droplet was calculated (see Table 2). Higher S_c values were obtained for smaller particles. This is due to the Kelvin effect, which is more pronounced for particles with higher curvature.

Figure 9 shows critical supersaturations obtained for the measurements at 1 kW load (with regular fuel) and at 2 kW load (with sulfur enhanced fuel). The

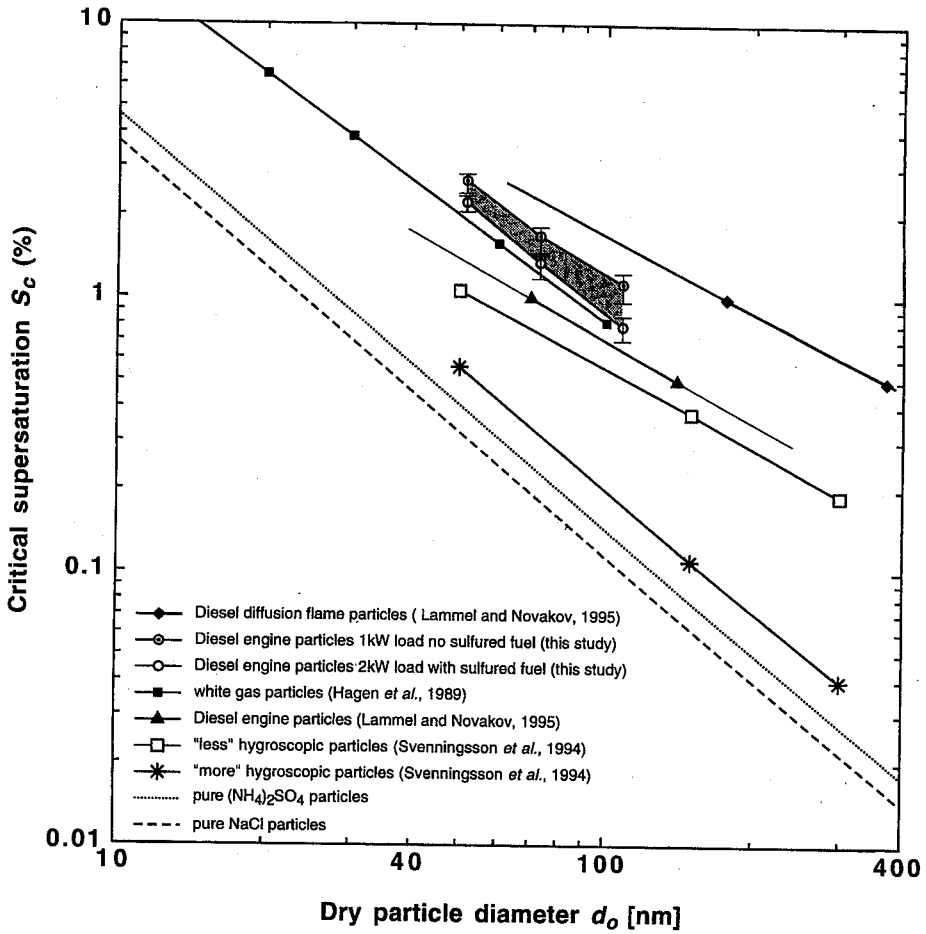

Fig. 9. Critical supersaturation spectra for freshly emitted combustion particles investigated in this study and for particles measured by other authors. Theoretical supersaturation spectra for pure NaCl and $(NH_4)_2SO_4$ particles as well as calculated spectra for less and more hygroscopic particles found in field experiments are also shown.

error bars were calculated by error propagation from the uncertainty determined for N_1. Critical supersaturation spectra for pure NaCl and $(NH_4)_2SO_4$ particles calculated with equation (3) are included for comparison. The hydration properties investigated in this study are also compared to measurements performed by other authors. Lammel and Novakov (1995) investigated the hygroscopicity of soot particles produced by two sources using diesel fuel. These were (a) an alcohol lamp in which the fuel was burnt in a diffusion flame and (b) an idling V8 Bus engine with mechanical injection. The condensation nuclei (CN) and cloud condensation nuclei (CCN) concentration of the monodisperse particles were measured simultaneously at constant supersaturations. An "activation radius" was defined as the dry particle radius for which 50% of all particles were activated. In Fig. 9 their results for diesel combustion aerosols from the vehicle engine and the diffusion flame are shown. The measurements on an idling diesel engine differ from the ones reported in this study where no hygroscopic growth was measured (see Fig. 7). This could be due to different engine types or different pre-treatment procedures. In the study of Lammel and Novakov (1995) the aerosol was stored in a bag and experienced a mean lifetime of 30 min. In a recent study (Weingartner *et al.*, 1995) combustion particles were also stored in a bag and it was observed that with increasing aging time the particles became more hygroscopic.

Hagen *et al.* (1989) exposed monodisperse particles produced by combustion of ethanol and white gas (with a blowtorch burner) to supersaturations. They found that the particles from the ethanol flame had higher critical supersaturations then the white gas particles (S_c was enhanced for 20 nm $< d_0 <$ 110 nm by about 2%). In Fig. 9 the regression lines given by the authors for white gas is included.

In field experiments in populated areas, where the hygroscopicity of the particles was also measured by means of a TDMA, two kinds of particles are commonly found, i.e. more hygroscopic and less hygroscopic particles (Covert and Heintzenberg, 1984; McMurry and Stolzenburg, 1989; Svenningsson

et al., 1992, 1994; Zhang *et al.*, 1993). In the study of Svenningsson *et al.* (1994) the measured hygroscopicity was compared to the growth of an insoluble particle containing ammonium sulfate $(NH_4)_2SO_4$. The volume fractions of $(NH_4)_2SO_4$ for the less hygroscopic particles were estimated to be 14, 4, and 2% for $d_0 = 50$, 150 and 300 nm, respectively. For the more hygroscopic particles the volume fractions were estimated to be 53, 48, and 52%, respectively. The corresponding supersaturations S_c necessary to activate the particles were calculated with equation (3) and found to be 1.06, 0.38, and 0.19% for the less hygroscopic particles and 0.56, 0.11, and 0.04% for the more hygroscopic particles, respectively. Since the measurements by Svenningsson *et al.* (1994) were performed in a populated area it can be expected that combustion generated particles are mainly present in the less hygroscopic mode. This hypothesis is consistent with recent findings of McMurry *et al.* (1996). In their paper the more and less hygroscopic atmospheric particles in populated area were sampled by means of a TDMA and analyzed. Carbon was mostly found in the less hygroscopic particles.

In contrast to the more and less hygroscopic atmospheric particles found in field experiments or to completely soluble NaCl or $(NH_4)_2SO_4$ particles the fresh diesel particles investigated in this study cannot act as CCN at supersaturations $S < 1\%$. Supersaturation in the atmosphere will normally not exceed 1% because droplet formation and growth on the present hydrophilic nuclei will consume the excess vapor and prevent other less soluble particles from becoming activated at higher supersaturations. The less hygroscopic mode will only be activated to a significant fraction in clouds with a relatively high peak supersaturation (Svenningsson *et al.*, 1994).

The question arises which aging processes are responsible for the observed hygroscopicity of soot particles in the field experiments. Possible mechanisms leading to an increase of the hygroscopicity of the soot particles are:

Coagulation in the atmosphere will transform the originally externally mixed aerosol towards an internal mixture where the soot is present together with salts, such as ammonium sulfate, in the same aerosol particle. In addition, particles will increase their size by coagulation and thus become better CCN. Since even in remote areas like Spitzbergen (Covert and Heintzenberg, 1993) an externally mixed aerosol was found, it must be hypothesized that coagulation processes do not efficiently transform the particles towards an internal mixture.

Gas-to-particle conversion may also change the hygroscopicity of atmospheric particles. Heterogeneous nucleation of condensable compounds—produced by chemical or photochemical transformations—can change the hygroscopicity of the particles. Andrews and Larson (1993) showed that the hygroscopicity of a carbon black particle was enhanced if it was coated with a hydrophilic organic surfactant (e.g. azelaic acid). Such surfactants adsorbed to an originally hydrophobic surface will preferentially put their hydrophilic part outwards and, thus increase the hygroscopicity of the particle. The inverse effect can occur if hydrophobic organic compounds adsorb and form a surface film which hinders transport of water into the particle (Saxena *et al.*, 1995).

Cloud processing is another important mechanism which will enhance the hygroscopicity of particles. In clouds the particles that do not act as CCN are present as interstitial particles between the droplets. Due to their Brownian diffusion the inactivated particles can be incorporated into droplets. Therefore, particles that are subjected to condensation and evaporation cycles can become more hygroscopic. Furthermore, the adsorption of soluble gases (e.g. SO_2, NO_2, HNO_2, HNO_3, NH_3) is enhanced on particles which are covered with a water layer. Especially if the particles are activated and thus have eminently increased their surface than they can gain large amounts of e.g. sulfate. Care has to be taken if organic films are adsorbed on the aqueous surfaces. Gill *et al.* (1983) showed that under these conditions the transfer of gases to the particles surfaces is considerably retarded.

Photochemical degradation of hydrocarbons by UV radiation will also increase the amount of hydrophilic and soluble compounds by an oxidation of the particle surface. The photooxidation of the particles is most probably dependent on the RH of the surrounding air. Kamens *et al.* (1988) found that the photoinduced decay of particle bound PAH is enhanced with increasing RH. A possible explanation given by the authors for this humidity effect is that OH radicals attack the particle surface. At higher RH a water layer is present on particles which might modify the accommodation coefficient of the OH radical. As seen from the experiments described above, the photooxidation of freshly emitted soot particles is accompanied with gas to particle conversion of soluble material.

The interactions of aerosol particles with RH are believed to be a cause for the uncertainty in climate forcing quantification. Therefore, the relative importance of the pathways which increase the hygroscopicity of aerosol particles in the atmosphere has to be evaluated by future experiments.

4. CONCLUSIONS

The hygroscopic growth of diesel soot particles and carbon particles was measured at subsaturations. Carbon particles did not show any condensational growth while diesel soot particles grew by 2.5% in diameter at 95% RH. With a Köhler model critical supersaturations S_c of the diesel particles were calculated, and S_c was found to be considerably higher than for pure NaCl or $(NH_4)_2SO_4$ particles. Thus, freshly emitted diesel soot particles are poor cloud condensation nuclei in the atmosphere. This however

is a result for freshly prepared particles, which is modified by aging effects. Addition of sulfur to the fuel as well as pre-treatment of the exhaust gas with ozone or UV radiation leads to a higher hygroscopicity of the particles. We suggest that a further aging in the atmosphere might lead to a higher hygroscopicity and thus to more efficient nucleation, as observed by other authors in field experiments.

Acknowledgements—We would like to express our gratitude to H. C. Siegmann and H. W. Gäggeler for their support and helpful suggestions. We also want to thank P. Walther from the Laboratory for EM1, Institute of Cell Biology, ETH Zürich for carrying out the electron microscopic analyses and S. Brütsch, who performed the chemical analyses. This work was supported by the AC Laboratorium Spiez.

REFERENCES

Andrews, A. and Larson, S. M. (1993) Effect of surfactant layers on the size changes of aerosol particles as a function of relative humidity. *Envir. Sci. Technol.* **27**, 857–865.

Bäcker, M. (1991) Untersuchungen zur Eignung des photoelektrischen Aerosolsensors als schnelle Messtechnik zur Bestimmung PAH-haltiger Partikeln im Abgas von Diesel- und Otto-Motoren. Dissertation, University Dortmund.

Burtscher, H., Matter, D. and Steiner, D. (1993) Characterization of soot particles by in situ measurement with different aerosol analysis tools. Report Series in Aerosol Science, *Finish Assoc. Aerosol Res.* **23**, 65–67.

Burtscher, H., Künzel, S. and Hüglin, C. (1995) Structure of particles in combustion engine exhaust. *J. Aerosol Sci.*, **26**, Suppl. 1, S129–S130.

Chughtai, A. R., Jassim, J. A., Peterson, J. H., Stedham, D. H. and Smith, D. M. (1991) Spectroscopic and solubility characteristics of oxidized soots. *Aerosol Sci. Technol.* **15**, 112–126.

Covert, D. S. and Heintzenberg, J. (1984) Measurements of the degree of internal/external mixing of hygroscopic compounds and soot in atmospheric aerosols. *Sci. Total Envir.* **36**, 347–352.

Covert, D. S. and Heintzenberg, J. (1993) Size distributions and chemical properties of aerosol at Ny Ålesund, Svalbard. *Atmospheric Environment* **27A**, 2989–2997.

Crouzet, Y. and Marlow, W. H. (1995) Calculations of the equilibrium vapor pressure of water over adhering 50–200 nm spheres. *Aerosol Sci. Technol.* **22**, 43–59.

Chylek, P. and Hallett, J. (1992) Enhanced absorption of solar radiation by cloud droplets containing soot particles in their surface. *Q. Jl. R. Met. Soc.* **118**, 167–172.

Dua, S. K. and Hopke, P. K. (1996) Hygroscopic growth of assorted indoor aerosols. *Aerosol Sci. Technol.* **24**, 151–160.

Fendel, W., Matter, D., Burtscher, H. and Schmidt-Ott, A. (1995) Interaction between carbon or iron aerosol particles and ozone. *Atmospheric Environment* **29**, 967–973.

Gill, P. S., Graedel, T. E. and Weschler, C. J. (1983) Organic films on atmospheric aerosol particles, fog droplets, cloud droplets, raindrops, and snowflakes. *Rev. Geophys. Space Phys.* **21**, 903–920.

Hagen, D. E., Trueblood, M. B., and White, D. R. (1989) Hydration properties of combustion aerosols. *Aerosol Sci. Technol.* **10**, 63–69.

Hansen, A. D. A., Rosen, H. and Novakov, T. (1984) The aethalometer—an instrument for the real-time measurement of optical absorption by aerosol particles. *Sci. Total Envir.* **36**, 191–196.

Hinds, W. C. (1982) *Aerosol Technology—Properties, Behavior, and Measurement of Airborne Particles.* Wiley, New York.

Jennings, S. G. (1988) The mean free path in air. *J. Aerosol Sci.* **19**, 159–166.

Jullien, R., Botet, R. and Mors, P. M. (1987) Computer simulations of cluster–cluster aggregation. *Faraday Discuss. Chem. Soc.* **83**, 125–137.

Kamens, R. M., Guo, Z., Fulcher, J. N. and Bell, D. A. (1988) The influence of humidity, sunlight, and temperature on the daytime decay of polyaromatic hydrocarbons on atmospheric soot particles. *Envir. Sci. Technol.* **22**, 103–108.

Kogelschatz, U. (1992) Silent-discharge driven excimer UV sources and their applications. *Appl. Surface Sci.* **54**, 410–423.

Köhler, H. (1936) The nucleus and the growth of hygroscopic droplets. *Trans. Faraday Soc.* **32**, 1152–1161.

Lammel, G. and Novakov, T. (1995) Water nucleation properties of carbon black and diesel soot particles. *Atmospheric Environment* **29**, 813–823.

Landau, L. D. and Lifshitz, E. M. (1993) *Fluid Mechanics, Course of Theoretical Physics*, 2nd Edn, Vol. 6. Pergamon Press, Oxford.

Matter, D., Mohr, M., Fendel, W., Schmidt-Ott, A. and Burtscher, H. (1995) Multiple wavelength aerosol photoemission by excimer lamps. *J. Aerosol Sci.*, **26**, 1101–1115.

McMurry, P. H. and Stolzenburg, M. R. (1989) On the sensitivity of particle size to relative humidity for Los Angeles aerosols. *Atmospheric Environment* **23**, 497–507.

McMurry, P. H., Litchy, M., Huang, P. -F., Cai, X., Turpin, B. J., Dick, W. D. and Hanson, A. (1996) Elemental composition and morphology of individual particles separated by size and hygroscopicity with the TDMA. *Atmospheric Environment* **30**, 101–108.

Myers, D. (1991) *Surfaces, Interfaces, and Colloids—Principles and Applications.* VCH Publishers, New York.

Nagatani, T., Saito, S., Sato, M. and Yamada, M. (1987) Development of an ultra high resloution scanning electron microscope by means of a field-emission source and in-lens system. *Scanning Microsc.* **1**, 901–909.

Needham, J. R., Doyle, D. M., Faulkner, S. A and Freeman, H. D. (1989) Technology for 1994. SAE paper 891949.

Nelson, J. A., Crookes, R. J. and Simons, S. (1990) On obtaining the fractal dimension of a 3D cluster from its projection on a plane — application to smoke agglomerates. *J. Phys. D* **23**, 465–468.

Press, W. H., Flannery, B. P., Teukolsky, S. A. and Vetterling, W. T. (1986) *Numerical Recipes — the Art of Scientific Computing*, pp. 523–528. University Press, Cambridge.

Pruppacher, H. R., Klett, J. D. (1980) *Microphysics of Clouds and Precipitation.* Reidel, Dordrecht.

Saxena, P., Hildemann, L. M., McMurry, P. H. and Seinfeld, J. H. (1995) Organics alter hygroscopic behavior of atmospheric particles. *J. geophys. Res.* **100**, 18,755–18,770.

Schleicher, B., Künzel, S. and Burtscher, H. (1995) *In-situ* measurement of size and density of submicron aerosol particles. *J. Appl. Phys.* **78**, 4416–4422.

Schwyn, S., Garwin, E. and Schmidt-Ott, A. (1988) Aerosol generation by spark discharge. *J. Aerosol Sci.* **19**, 639–642.

Shulman, M. L., Jacobson, M. C., Charlson, R. J., Synovec, R. E. and Young, T. E. (1996) Dissolution behavior and surface tension effects of organic compounds in nucleating cloud droplets. *Geophys. Res. Lett.* **23**, 277–280.

Steiner, D., Burtscher, H. and Gross, H. (1992) Structure and disposition of particles from a spark-ignition engine. *Atmospheric Environment* **26A**, 997–1003.

Steiner, D. (1993) Physik der Verbrennungspartikel. Dissertation ETH Zürich No. 10191.

Svenningson, I. B., Hansson, H.-C., Wiedensohler, A., Ogren, J. A., Noone, K. J. and Hallberg, A. (1992) Hygroscopic growth of aerosol particles in the Po Valley. *Tellus* **44B**, 556–569.

Svenningsson, I. B., Hansson, H.-C., Wiedensohler, A., Noone, K. J., Ogren, J. A., Hallberg, A., and Colvile, R. (1994) Hygroscopic growth of aerosol particles and its influence on nucleation scavenging in clouds: Experimental results from Kleiner Feldberg. *J. Atmos. Chem.* **19**, 129–152.

Twomey, S., Piepgrass, M. and Wolfe, T. L. (1984) An assessment of the impact of pollution on the global cloud albedo. *Tellus* **36B**, 356–366.

Weber, A. P., Baltensperger, U., Gäggeler, H. W. and Schmidt-Ott, A. (1996) *In situ* characterization and structure modification of agglomerated aerosol particles. *J. Aerosol Sci.* **27**, 915–929.

Weingartner, E., Baltensperger, U. and Burtscher, H. (1995) Growth and structural change of combustion aerosol at high relative humidity. *Envir. Sci. Technol.* **29**, 2982–2986.

Weller, S. and Young, T. F. (1948) Oxygen complexes on charcoal. *J. American Chem. Soc.* **70**, 4155–4162.

Zhang, X. Q., McMurry, P. H., Herring, S. V. and Casuccio, G. S. (1993) Mixing characteristics and water content of submicron aerosols measured in Los Angeles and the Grand Canyon. *Atmospheric Environment* **27A**, 1593–1607.

APPENDIX

For our application, a change of RH in the second DMA has a small but important influence on the characteristics of this instrument. In our set-up the sheath and excess air flow rates as well as the mean free path λ, the dynamic viscosity η and the density ρ of the air are dependent on temperature T and RH.

The following empirical formulas for λ, η and ρ for air at 1010 mbar were calculated by interpolating the data reported by Jennings (1988).

$$\lambda = (1.3333 \times 10^{-12}\ \mathrm{RH} + 3.1421 \times 10^{-10}(T - 20) + 6.5385 \times 10^{-8})\ \mathrm{m} \quad \text{(A1)}$$

$$\eta = (-5.7666 \times 10^{-10}\ \mathrm{RH} + 5.2947 \times 10^{-8}(T - 20) + 1.8187 \times 10^{-5})\ \mathrm{kg\,(m\,s)^{-1}} \quad \text{(A2)}$$

$$\rho = (-1.2267 \times 10^{-4}\ \mathrm{RH} - 4.4009 \times 10^{-3}(T - 20) + 1.2054)\ \mathrm{kg\,m^{-3}} \quad \text{(A3)}$$

where T is in °C and RH in %.

The accuracy of these empirical formulas are better than 0.15% for 0% < RH < 100% and 20°C < T < 25°C.

The electrical mobility Z_p of a particle with mobility diameter d_p is dependent on λ and η by the following relations:

$$Z_p = \frac{n_p\ e\ C}{3\,\pi\,\eta\,d_p} \quad \text{(A4)}$$

where

$$C = 1 + 1.257\left(\frac{2\ \lambda}{d_p}\right) + 0.4\left(\frac{2\ \lambda}{d_p}\right)\exp\left(\frac{-1.1 d_p}{2\ \lambda}\right) \quad \text{(A5)}$$

is the Cunningham slip correction (Hinds, 1982) n_p = number of elementary charges on the particle (in our application = 1); e = elementary charge = 1.602×10^{-19} C.

Furthermore, a change in RH (and T) has an influence on the relation between Z_p and the voltage on the center electrode U

$$U = \frac{0.5\ (q_V^S + q_V^E)\ \ln\left(\frac{r_2}{r_1}\right)}{2\,\pi\,l\,Z_p} \quad \text{(A6)}$$

where r_1, r_2 is the inner and outer electrode radius, respectively, l the effective DMA length, q_V^S, q_V^E the sheath and excess air volume flow rates, respectively.

The sheath air is humidified after a mass flow controller with a mass flow rate of q_m^{FC}. Therefore, q_V^S can be expressed as

$$q_V^S = \frac{1}{\rho}\left(q_m^{FC} + \frac{d}{dt}\,m_{H_2O}\right) \quad \text{(A7)}$$

with

$$\frac{d}{dt}\,M_{H_2O} = \frac{d}{dt}\,\frac{M_{H_2O}\,p_{H_2O}\,V}{RT} = \frac{M_{H_2O}\,p_{H_2O}}{RT}\,\frac{1}{\rho_0}\,q_m^{FC} \quad \text{(A8)}$$

where m_{H_2O} is the mass of water which is added to a volume V by the humidifier, M_{H_2O} the molecular weight of water, R the gas constant, ρ_0 the density of dry air at temperature T and p_{H_2O} the partial pressure of the water vapor, which can be approximated with the empirical formula:

$$p_{H_2O}\,(\mathrm{mbar}) = \frac{\mathrm{RH}}{100\%}\,6.108\,\exp\left(5350\left(\frac{1}{273.15} - \frac{1}{T + 273.15}\right)\right) \quad \text{(A9)}$$

where T is in °C.

In our setup the excess air flow is controlled with a critical orifice, where the volume flow is given by (Landau and Lifshitz, 1993):

$$q_V^E = \frac{1}{\rho}\,S\,\sqrt{2\ p\ \rho}\left(\frac{2}{\chi + 1}\right)^{1/(\chi - 1)}\sqrt{\frac{\chi}{\chi + 1}} \quad \text{(A10)}$$

where χ is the c_p/c_v, S = smallest cross section area of the orifice, p = total pressure inside TDMA (= 1010 mbar) and c_p, c_v = specific heat constant for constant pressure and volume, respectively.

By assuming an ideal gas, χ is expressed by

$$\chi = (\alpha\ c_p^{Air} + \beta\ c_p^{H_2O})/(\alpha\ c_v^{Air} + \beta\ c_v^{H_2O}) \quad \text{(A11)}$$

where

$$\alpha = 1 - \frac{p_{H_2O}\ [\mathrm{mbar}]}{1010\ \mathrm{mbar}},\ \beta = \frac{p_{H_2O}\ [\mathrm{mbar}]}{1010\ \mathrm{mbar}},$$

$c_p^{Air} = 7/2\ R$, $c_v^{Air} = 5/2\ R$, $c_p^{H_2O} = 4\ R$ and $c_v^{H_2O} = 3\ R$.

A calculation, which takes into account that a change in RH leads to a change of λ, η and ρ equations (A1)–(A3) and also to a change in the sheath and excess air flows equations (A7) and (A10) was performed for ambient temperature (20°C). An evaluation showed that the effect of the RH on the DMA characteristic can be described very well for 50 nm < d_p < 110 nm by the following empirical correction:

$$\frac{d_p^{real}}{d_p^{measured}} = 1 - c\ \mathrm{RH}\ [\%],\ \text{with}\ c = 6.5 \times 10^{-5} \pm 0.3 \times 10^{-5} \quad \text{(A12)}$$

where d_p^{real} denotes the real mobility diameter calculated with consideration of RH and $d_p^{measured}$ the mobility diameter calculated with equations (A4) and (A6) for dry air.